Geophysical Journal (1988) **92**, 253–267

Source mechanisms of moderate-size earthquakes and stress orientation in mid-plate South America

Marcelo Assumpção
Depto. de Geociências, Universidade de Brasília, 70910 Brasília, Brazil

Gerardo Suárez*
Lamont-Doherty Geological Observatory, Palisades, 10967 New York, USA

Accepted 1987 July 6. Received 1987 July 6; in original form 1986 June 26

SUMMARY

Fault plane solutions of six mid-plate earthquakes with magnitudes ranging from 4.8 to 5.5 m_b were determined using *P*-wave first motion data and the relative amplitudes of short-period teleseismic depth phases (pP and sP). These results, together with previous studies, show a predominance of reverse and strike–slip faulting indicating horizontal compressional stresses in mid-plate South America. The orientation of the *P*-axes, however, is not uniform. In western and southwestern Brazil the *P*-axes are oriented approximately E–W (probably due to the Nazca–South America plate convergence). In eastern Brazil the direction of the *P*-axes show more scatter, but an average E–W direction is consistent with the available data. On the contrary, in northern Brazil, the *P*-axes of two events in the Amazon basin trend approximately N–S, a direction perpendicular to the direction of absolute plate motion as well as to the relative plate motions Nazca–South America and South America–Africa.

Key words: fault plane solution, intraplate seismicity, stress, South America

1 INTRODUCTION

The orientation of regional lithospheric stresses in intraplate regions has been frequently used to infer the driving forces that cause plate motions in the Earth's surface (e.g. Mendiguren 1971; Richardson *et al.* 1976, 1979; Bergman & Solomon 1980; Wiens & Stein 1985). The state of stress in the lithosphere can be due to a variety of forces caused both by local sources (e.g. stress concentrations due to structure heterogeneities, crustal loading and unloading, asthenospheric thermal anomalies) and by regional, more uniform sources related to plate motion (such as ridge-push, negative buoyancy of the subducted lithosphere and viscous shear forces in the lithosphere–asthenosphere boundary). Although it is not always easy to distinguish between local and regional sources of stress, it is usually thought that plate tectonic forces play a major role in determining the stress field in mid-plate regions. This is revealed by the consistency of stress indicators (earthquake mechanisms, *in situ* stress measurements and stress-sensitive geological features) over large intraplate areas (Richardson *et al.* 1979; Zoback & Zoback 1980).

Focal mechanisms of intraplate earthquakes are the tools most commonly used to infer the orientation of the regional tectonic stress field (Richardson *et al.* 1979; Bergman & Solomon 1984). However, a large number of events are necessary to establish the regional stress field, not only because local sources need to be averaged out, but also because intraplate events tend to occur on pre-existing zones of weakness and reactivated faults (Sykes 1978; Bergman & Solomon 1980) in which case the stresses released by the earthquake (i.e. the *P* and *T*-axes of the fault plane solution) may not coincide with the regional lithospheric stresses (McKenzie 1969).

The regional lithospheric stresses in Brazil have been tentatively inferred by Mendiguren & Richter (1978) and Assumpção *et al.* (1985) through the study of earthquake focal mechanisms. The state of knowledge about the stresses in the middle of the South America plate, however, remains poor because of the small number of events available. Furthermore, the small-to-moderate magnitudes of the mid-plate events available for such studies do not always allow the focal mechanism to be well constrained.

The purpose of this paper is to present some additional focal mechanism solutions and depths (Fig. 1 and Table 1) in order to increase the basic data set upon which better inferences about the state of stress in the middle of the South America plate can be made. One earthquake studied by Mendiguren & Richter (1978) is re-analysed, and the focal mechanisms of four additional events ($m_b = 5$) are determined using not only *P*-wave polarity data, but also the relative amplitudes of the direct *P* and surface reflection phases pP and sP.

The result of this analysis (Table 1 and Fig. 1) shows that

* Present address: Instituto de Geofisica, Universidad Nacional Autônoma de México, Cd. Universitaria, México 04510, D.F.

Figure 1. Orientation of *P*-axes of Brazilian earthquakes and other mid-plate events near Brazil. Event numbers refer to Table 1. Events of predominantly thrust or normal faulting are represented by the *P*- or *T*-axis, respectively. Strike-slip events are represented by both the *P* and *T* axes. Convergent and divergent arrows indicate the respective directions of the *P*- and *T*-axes. Filled arrow heads indicate directions with estimated uncertainties less than ±20°; open arrowheads, uncertainties greater than ±20°. The two events numbered 7 and 8 are composite focal mechanisms of reservoir-induced events.

Table 1. Focal mechanism parameters of the events in Fig. 1.

No.	Date	h min s	Lat. (°)	Long. (°)	Depth§ (km)	m_b	Fault plane sol. strike	dip	slip	*P*-axis strike/dip	*T*-axis strike/dip	References
01	31 Jan 55	05:03:07	−12.42	−57.30	N	6.2*	53	49	92	142/04	342/86	Mendiguren & Richter 1978
02	01 Mar 55	01:46:18	−19.84	−36.75	N	6.1*	07	52	130	250/00	341/86	Mendiguren & Richter 1978
03	14 Dec 63	00:05:42	−02.30	−61.01	45	5.1	243	52	96	329/07	184/82	this paper
04	13 Feb 64	11:21:46	−18.06	−56.69	5	5.4	130	60	37	254/01	345/46	this paper
05	27 Aug 68	05:17:36	−08.90	−72.89	26	4.9	240	48	157	107/15	212/43	this paper
06	27 Sep 74	04:09:02	+02.72	−71.37	6	5.5	59	87	185	285/05	195/02	Suárez *et al.* 1983
07	1976	swarm†	−20.2	−44.7	1	<3.5	200	74	72	304/27	86/57	Mendiguren & Richter 1978
08	1977–78	swarm‡	−23.4	−45.6	1	<2.5	‡	‡	‡	45/02	variable	Mendiguren 1980
09	06 Mar 80	09:46:18	−06.17	−71.16	18	4.8	134	41	95	40/04	182/85	this paper
10	12 Nov 80	21:23:05	−08.07	−50.24	N	4.7	134	63	−52	93/55	197/10	Assumpção *et al.* 1985
11	20 Nov 80	03:29:42	−04.30	−38.40	5	5.2	244	88	182	109/03	199/00	Assumpção *et al.* 1985
12	08 Apr 82	05:58:52	−24.80	−58.10	12	4.9	126	88	−1	81/03	351/01	this paper
13	05 Aug 83	06:21:42	−03.59	−62.17	23	5.5	305	60	120	14/10	264/62	this paper

* Approximate magnitude based on PAS, PAL and OTT short-period records.
† Composite solution of reservoir induced events.
‡ Four different composites of reservoir induced events, two reverse and two strike-slip mechanisms; *T*-axis is variable but the *P*-axis is approximately constant.
§ Depths based on $pP-P$ difference using a Herrin model (except events 7 and 8).

the axes of maximum compression (*P*-axis) are nearly always horizontal. The orientation of the *P*-axes, however, varies substantially across South America. These different orientations may be useful in assessing the importance of the various plate tectonic forces acting on the South America plate boundaries.

2 FAULT PLANE SOLUTIONS FROM RELATIVE AMPLITUDE OF DEPTH PHASES

Some events in Brazil with focal depths between 10 and 45 km have produced clear short-period pP and sP phases at teleseismic distances, well separated from the direct *P*-wave. These events, having magnitudes around 5 m_b, are not usually recorded by a sufficient number of stations to have their nodal planes reliably determined with *P*-wave polarities alone. Pearce (1977, 1980) has shown that the amplitude information of the short-period depth phases can be extremely useful to constrain the possible orientations of the nodal planes. A procedure was established to determine the nodal planes using the amplitude information of the depth phases, in addition to the *P*-wave polarity. A computer program (PPSP) searches the nodal plane orientation that best fits the observed ratios of pP/P, sP/P and pP/sP amplitudes.

The theoretical amplitudes for the *P*- and *S*-waves at the source were calculated using a double couple model. Surface reflection coefficients were calculated using the simple half-space model for the crust. The program uses one *P*-wave velocity at the source to determine the take-off angles at the hypocentre, and another *P*-wave velocity for the half-space to model the surface incidence angle and reflection coefficients. A Poisson's ratio of 0.25 was used. No differential inelastic attentuation between *P* and *pP* or *sP* was included in the program because the depths involved were not large enough (maximum depth of 45 km). The difference in geometrical spreading factors between *P* and *sP* was taken into account.

At each station, the observed ratio to be fitted by the fault plane solution was chosen so that it was always less than or equal to one. That is, for any given station, the ratio pP/P was chosen if the observed *pP* amplitude was smaller than *P*; otherwise the ratio P/pP was the type of ratio to be modelled. The same criteria were applied to sP/P and pP/sP ratios. Changing the type of ratio so that it is always less than or equal to 1 has the advantage that when *P* (or *pP*) are very small compared to *pP* (or *P*) the ratio will be close to 0 and it is not critical that the sign of the weak phase be correctly identified. Also, when one of the nodal planes is close to a given station, the theoretical value for the ratio will not diverge but will tend to zero, making the solution more stable. Amplitudes of *P* and *pP* could be positive (i.e. compressional motion) or negative (dilation). Only the absolute values of the ratios sP/P and pP/sP were considered because it is usually very difficult to identify the direction of *sP* first motion.

The residuals of the amplitude ratios were defined as follows:

$$\mathrm{RES}(pP/P) = \mathrm{O}(pP/P) - \mathrm{T}(pP/P),$$

where

$$\mathrm{O}(pP/P) = \text{observed} \quad pP/P \quad \text{if} \quad pP < P, \quad \text{or}$$

$$= \text{observed} \quad P/pP \quad \text{if} \quad pP > P,$$

and

$$\mathrm{T}(pP/P)$$

$$= \text{theoretical} \quad pP/P \quad \text{if observed} \quad pP < \text{observed} \quad P, \quad \text{or}$$

$$= \text{theoretical} \quad P/pP \quad \text{if observed} \quad pP > \text{observed} \quad P.$$

The nodal planes were chosen as the ones giving the smallest residuals in the least-squares sense, i.e. giving the minimum standard deviation, σ, defined as:

$$\sigma^2 = 1/(N-3)\sum[(\mathrm{RES}(pP/P))^2 + (\mathrm{RES}(sP/P))^2 + (\mathrm{RES}(pP/sP))^2],$$

where *N* is the total number of ratios (one or three per station).

Although this procedure of searching in the whole parameter space for the absolute minimum σ allows the best solution to be obtained, it is not easy to estimate the uncertainties of the fault plane solution (fps). A preliminary estimate of the confidence limits of the fps was obtained by using the *F* test. Calling σ_0 the minimum standard deviation of the adopted best solution, the 'confidence limits' were defined by including all other fps with σ such that the *F* ratio (i.e. σ^2/σ_0^2) would be below the 95 per cent probability level of the *F* distribution with $N-3$ degrees of freedom. This is not an accurate statistical procedure because the basic observations (amplitude ratios) do not follow a Gaussian distribution. However, before a more appropriate statistical procedure is developed, this so called '95 per cent confidence limit' may be useful as a preliminary guide to assess the reliability of the fault-plane solutions presented, especially regarding the orientation of the *P*-axis.

After finding the best-fitting orientation of the nodal planes, synthetic seismograms were calculated to check the PPSP solution.

2.1 Test of PPSP program with the CODAJÁS event (No. 13 in Fig. 1)

The fault plane solution of this event in the Amazon Basin is well defined by many clear compressional first motions at teleseismic distances and a few clear dilations recorded at regional stations (Fig. 2a). With a depth of 23 km, *pP* and *sP* phases are well separated in the short-period records (Fig. 2c) so that a test of the amplitude ratio method could be performed. A *P*-wave velocity of 6.8 km s^{-1} at the source and a half-space velocity of 5.5 km s^{-1} were used in the program. Fig. 2(b) shows the fault-plane solution obtained with the program PPSP using only 10 stations. These stations were selected at random from a total of 41 teleseismic stations with the condition that they covered the widest range of epicentral distances (44° to 91°) and azimuths. The PPSP solution (Fig. 2b) is very close to the previous solution (Fig. 2a) obtained with all polarity data. If all 41 teleseismic stations are used in PPSP, even without the dilatational first motions at regional distances, the solution (strike = 305, dip = 60, slip = 120 and $\sigma = 0.24$) is even closer to the one of Fig. 2(a).

2.1.1 Synthetic seismograms

Synthetic seismograms were calculated and compared with the observed traces to check the fault plane solutions given by the PPSP program. This was done in two ways. First, a half-space crustal model and a triangular source time function were used with the technique of Langston & Helmberger (1975). Similarly to the PPSP program, two different *P*-wave velocities were used in the crustal model: one for the source and another one for the surface reflections. In a second approach, the response of a layered crustal structure at the source was used instead of the half-space. In this case a program developed by Nábělek (1984) was used which allows the best source-time function to be calculated. At the stations simple half-space models were used in both cases. Upper-mantle attenuation was modelled with t^* values ranging from 0.3 to 0.5, according to the propagation paths (Lay & Helmberger 1981; Der *et al.*, Cormier 1982).

Figure 2(c) shows the synthetic seismograms of the Codajás event computed for two representative stations. Almost no information is available on Brazilian crustal structure, so a Herrin model was used with an added low-velocity sedimentary layer and some other slight modifications to match the synthetics better with the observed seismograms (Table 2). It can be seen from Fig. 2(c) that the synthetics calculated with the PPSP fault-plane solution match the

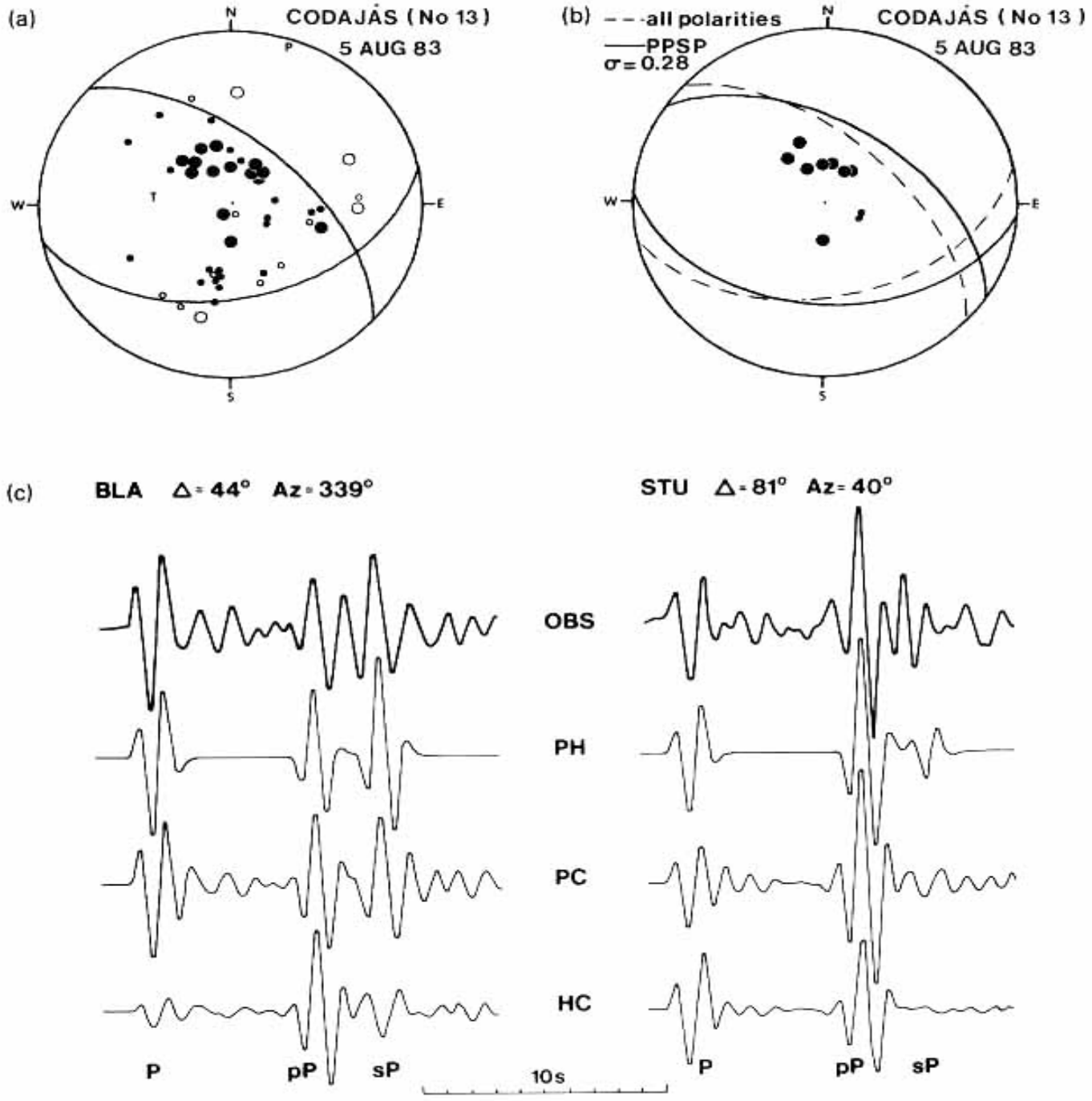

Figure 2. Fault plane solution of Codajás event (No. 13) of 5 August 1983 in the Amazon Basin. (a) Solution using all *P*-wave first motion data from teleseismic and regional stations (Assumpção *et al.* 1985). Closed symbols are compressional first motions, open symbols dilational; large and small symbols are more and less reliable polarities. (b) Solution obtained with only 10 teleseismic stations using depth-phases amplitude ratios with program PPSP (continuous line) compared with solution (a) (dashed line). Symbols as in Fig. 2(a). (c) Comparison of synthetic seismograms with the observed (top) traces. PH = synthetics computed with PPSP fault plane solution and a half-space crustal model; PC = synthetics with PPSP solution and a layered crustal model; HC = Harvard solution with a layered crustal model.

Table 2. Source crustal models used in the synthetic seismograms.

Codajás 1983				Manaus 1963				Acre 1980			
Depth (km)	α (km/s)	β	ρ (g/cm^3)	Depth (km)	α (km/s)	β	ρ (g/cm^3)	Depth (km)	α (km/s)	β	ρ (g/cm^3)
2	4.5	2.5	2.5	2	5.0	2.7	2.7	4	5.0	2.8	2.7
14	6.0	3.6	2.8	15	6.0	3.3	2.8	13	6.0	3.5	2.8
39	6.8	4.1	3.0	40	6.8	3.8	3.0	40	6.8	3.9	3.0
—	8.1	4.7	3.3	—	8.1	4.7	3.3	—	8.1	4.7	3.3

observed seismograms reasonably well (i.e. pP and sP amplitudes comparable to P for North American Stations; large pP and small sP for European stations) both with the half-space model and with the layered crustal structure. Although a layered crust produces more realistic-looking seismograms, the lack of information about the crust in the Amazon makes this better resemblance of doubtful significance. In any case, the PPSP search, using the two-velocity half-space model, can find a fault-plane orientation close enough to the final solution that could be obtained with a known crustal structure.

A moment tensor inversion for this event was made by Harvard University and published in the ISC bulletin. This kind of analysis (Dziewonski & Woodhouse 1983), using long-period body waves (mainly *SS* and *SSS*) with a low pass filter of 45 s, produced a reverse fault mechanism with the P-axis oriented E–W, in disagreement with the solution of Fig. 2(a). Also, the Harvard solution does not correctly reproduce the relative amplitudes of the short-period depth phases (Fig. 2c). The records of this earthquake, which had an $M_s = 4.5$ and a seismic moment of about 1×10^{24} dyn cm, close to the threshold ($M_s = 5.0$ and $M_0 = 1$ to 2×10^{24} dyn cm) of applicability of the Centroid Moment Tensor inversion (Dziewonski & Woodhouse 1983), were found to be contaminated by another bigger event that had occurred about one hour earlier in the Pacific region (Ekström 1987 private communication). The agreement of the two independent solutions presented here, one with P-wave polarities (Fig. 2a) and the other with amplitudes of depth phases (Fig. 2b, c), confirms the NNE orientation of the P-axis to be the correct one.

Although one event is not enough for a complete assessment of the realiability of the method of depth phases amplitude ratios used here, it does show that, given a reasonably good distribution of stations, and records with good signal-to-noise ratios, the correct nodal plane solution can be obtained using only teleseismic stations that would otherwise not allow the nodal planes to be constrained by first-motion polarities alone.

2.2 Manaus earthquake, Dec. 14 1963 (No. 3)

The Manaus event occurred near the northern edge of the Amazon sedimentary basin at a depth of 45 km. Clear first motions observed at only a few stations were not enough to constrain the fault-plane solution. The teleseismic records, however, show that the P signal was consistently similar on all stations that have steep take-off angles when they are aligned relative to the pP phase (Fig. 3a). Furthermore, applying a correction to the arrival-time differences between P and pP due to the different epicentral distances, the similarity of the direct P-wave at stations in North America, Europe, Africa and Antarctica becomes more apparent (Fig. 3b). The similarity of the P waveforms at stations with greatly different azimuths suggests that all these stations (Fig. 3b) are in the same lobe of radiation. The best stations (i.e. those with higher gains and higher signal-to-noise ratios) show that this event seems to be preceded by a small precursor with compressional first motion (Fig. 3c). Thus, we extrapolate the polarity of the other stations in Fig. 3(b) to be compressional.

The result of PPSP (Fig. 4a) shows a reverse fault with P-axis oriented approximately NNW. It is interesting to note that the solution satisfies the dilation at LPB even though it was not used as a constraint in the PPSP solution. This dilation at LPB (at a distance of 16°) is probably near a nodal plane because of the secondary very large phase, in agreement with the focal mechanism. Fig. 4(b) shows the synthetic seismograms for some of the WWSSN stations at different distances and azimuths. The synthetics were computed with Nábělek's (1984) technique using the PPSP fault-plane solution but allowing the best-fitting source-time function to be determined. No directivity was allowed, and a single-point source event was considered. In this case, what seemed to be a small precursor was actually modelled as a more gradual beginning of the source-time function. It can be seen that the PPSP solution reproduces the major features of the relative amplitudes of the P, pP and sP phases.

Although no measurement of crustal thickness is available for the Amazon Basin, the hypocentral depth of 45 km (from $pP-P$ times) seems to be greater than the average 35–40 km crustal thickness of shield areas (e.g. Godlewski & West 1977; Korhonen & Porkka 1981; Finlayson *et al.* 1984). For this reason the Manaus event of 1963 was taken to have occurred below the Moho and a source P-wave velocity of 8.1 km s^{-1} was used in the PPSP program. It is interesting to note that if a source velocity of 7.0 km s^{-1}, more typical of a lower crustal layer, is used, the best solution has a higher standard deviation of 0.44. This gives support to the assumption that the hypocentre lies just below the Moho as it seems to be in the majority of the deeper intraplate earthquakes in old continental areas (Chen & Molnar 1983).

2.3 Mato Grosso Do Sul, February 13 1964 (No. 4)

Mendiguren & Richter (1978) proposed a reverse fault mechanism for this earthquake based on P-wave polarities alone. Their solution, however, allows for a wide range of possible orientations of the P-axis. An examination of the

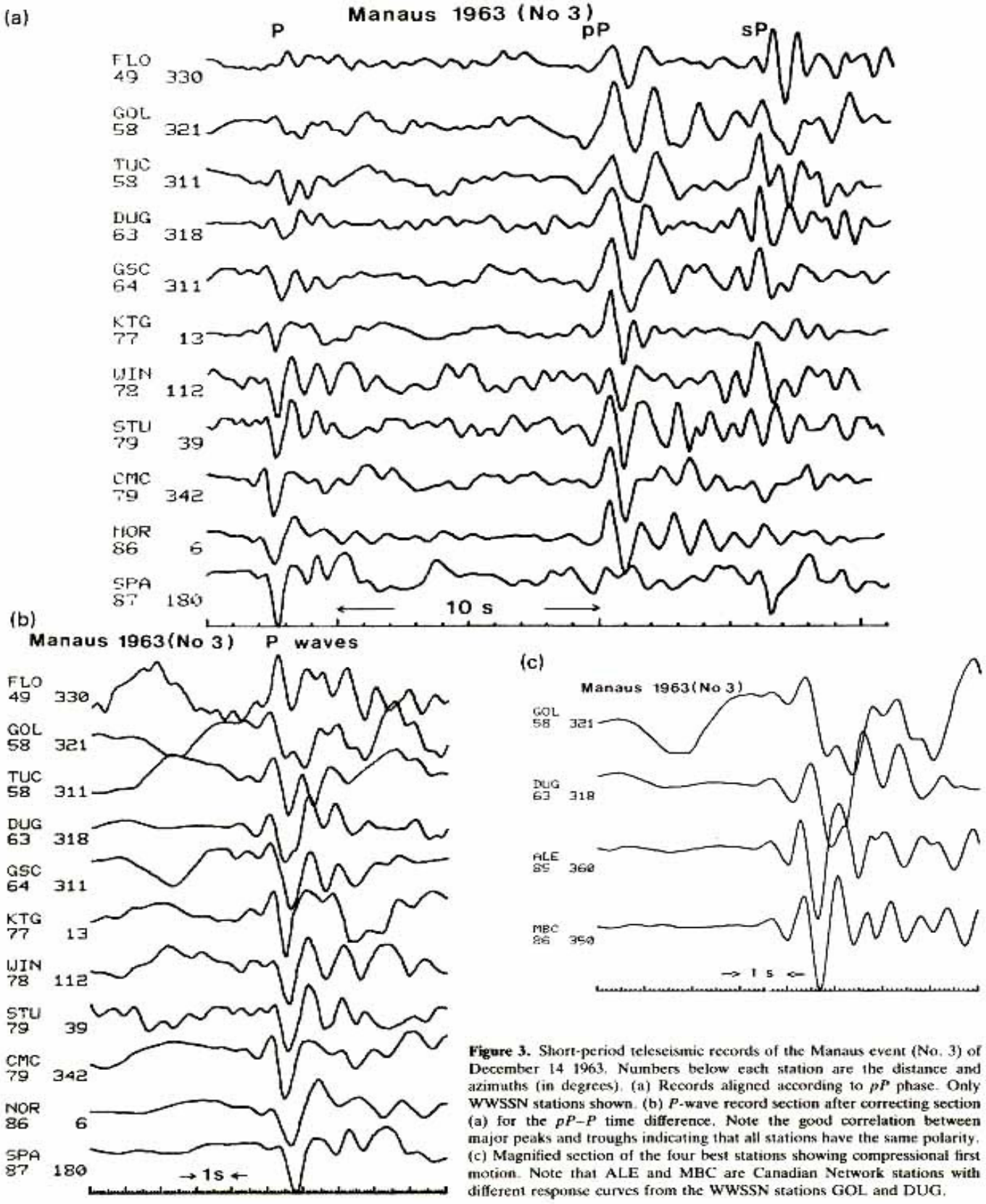

Figure 3. Short-period teleseismic records of the Manaus event (No. 3) of December 14 1963. Numbers below each station are the distance and azimuths (in degrees). (a) Records aligned according to *pP* phase. Only WWSSN stations shown. (b) *P*-wave record section after correcting section (a) for the *pP*–*P* time difference. Note the good correlation between major peaks and troughs indicating that all stations have the same polarity. (c) Magnified section of the four best stations showing compressional first motion. Note that ALE and MBC are Canadian Network stations with different response curves from the WWSSN stations GOL and DUG.

teleseismic records of this event (Fig. 5) shows that its depth is very shallow (about 5 km) and the depth phases are not separated, so it is not possible to use the method of depth-phases amplitude ratios. Short-period synthetic seismograms (with the two-velocity half-space model) were calculated for various nodal plane orientations and compared with the observed seismograms on a trial and error basis. In an attempt to improve the signal-to- noise ratio, stations that were very close together in the focal hemisphere were stacked. Because of the large fluctuations in amplitudes of short-period *P*-waves caused by variations in upper mantle and crustal structures at the source and receiver, only the shape, relative amplitudes and relative arrival times of the waveforms were modelled.

For this Mato Grosso event all clear teleseismic ($\Delta > 40°$) *P*-waves are compressional, indicating a predominantly reverse fault mechanism. Unfortunately no good records from local or regional stations exist to help constrain the strike of the nodal planes. Assuming the negative polarities at some South American stations (distant between 10° and 20°) were correctly identified, the synthetic seismograms show that the best nodal plane solution is a reverse fault with ENE-oriented *P*-axis (Fig. 5).

2.4 Acre, August 27 1968 (No. 5)

Figure 6(a) shows the PPSP fault plane solution for the Acre event obtained with 11 teleseismic stations ($\sigma = 0.31$). The data from regional stations do not show reliable polarities to constrain the nodal planes better. Synthetic seismograms with the half-space model were calculated, with the PPSP solution (Fig. 6b) showing good agreement with observations.

2.5 Western Amazon March 6 1980 (No. 9)

Figure 7(a) shows some of the teleseismic *P*-waves for this event which occurred in the western part of the Amazon sedimentary basin. It shows compressional first motion for the direct *P*-wave, and opposite polarity for the large depth phase, interpreted as *pP*. This is seen most clearly in the stations DUG and SPA. This interpretation indicates a reverse-fault mechanism (Fig. 7b). The hypothesis that the large depth phase is *sP* instead of *pP* is highly unlikely because the best nodal plane orientation, under that interpretation, would have a high standard deviation of 0.53 compared to 0.18 for the reverse-fault hypothesis. Figure 7(c) shows the synthetic seismograms for the three stations with best signal-to-noise ratio calculated with a layered crustal model and the PPSP fault plane solution of Fig. 7(b). If the weak dilation at ZOBO (Fig. 7b) is used as a constraint, the strikes of the nodal planes change by about 20° (the *P*-axis direction changes from NE to NNE). The two solutions are not significantly different (standard deviations of 0.18 and 0.21 respectively). This uncertainty in the strikes of the nodal planes is typical of purely reverse-fault earthquakes studied mainly with teleseismic data.

2.6. Paraguay earthquake, April 8 1982 (No. 12)

The teleseismic records of this event are very poor (Fig. 8). In order to improve the signal-to-noise ratio, records from stations that plotted close to one another in the focal hemisphere were stacked with the assumption that differences in signal shape between stations (due to differences in t^*, receiver structure and instrument

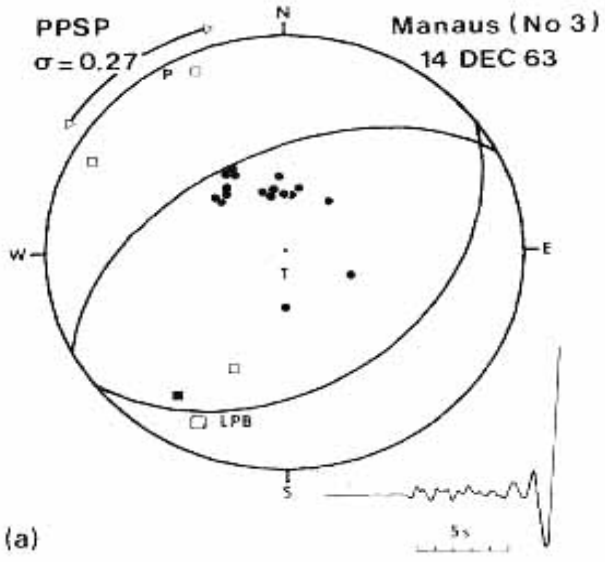

Figure 4. (a) Fault plane solution of Manaus event (No. 3). Circles are the teleseismic stations used in the PPSP program. Squares are polarity data not used as constraints in the PPSP solution. Symbols as in Fig. 2(a). The arrows outside the projection circles are an estimate of the 'confidence limits' of the *P*-axis direction. The dilation at LPB was not used as a constraint in the estimate of the *P*-axis uncertainty. (b) Comparison of synthetic (dashed lines) with observed (solid lines) seismograms.

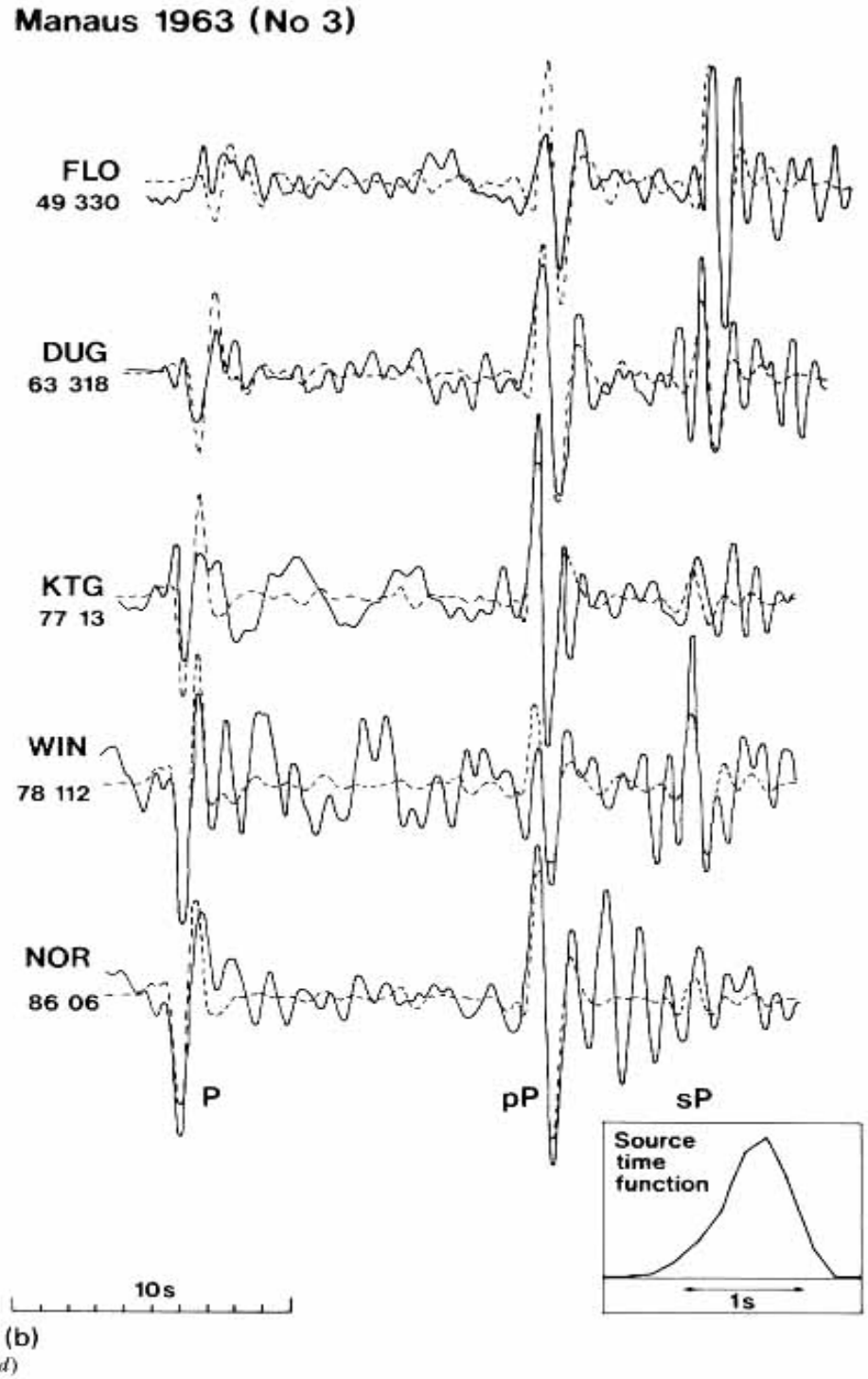

Figure 4. (*Continued*)

response) were not important compared with the station noise. Fig. 8(a) shows the two best records from the Canadian Network summed after alignment for best correlation of the *P*-wave signal. Fig. 8(b) shows the three best records from North American WWSSN stations. For these stations the *P*-waves in Fig. 8(b) were aligned according to the expected arrival times after corrections for station residuals were applied. These corrections were obtained by determining the relative residuals between the stations ALQ, GOL and DUG for three other well recorded Brazilian events: Manaus 1963 Dec. 14, Mato Grosso 1964 Feb. 13 and Codajás 1983 Aug. 5. These time corrections applied to the theoretical Jeffreys–Bullen arrival times in Fig. 8(b) (ALQ = 0.00, GOL = +0.45 and DUG = +0.71),

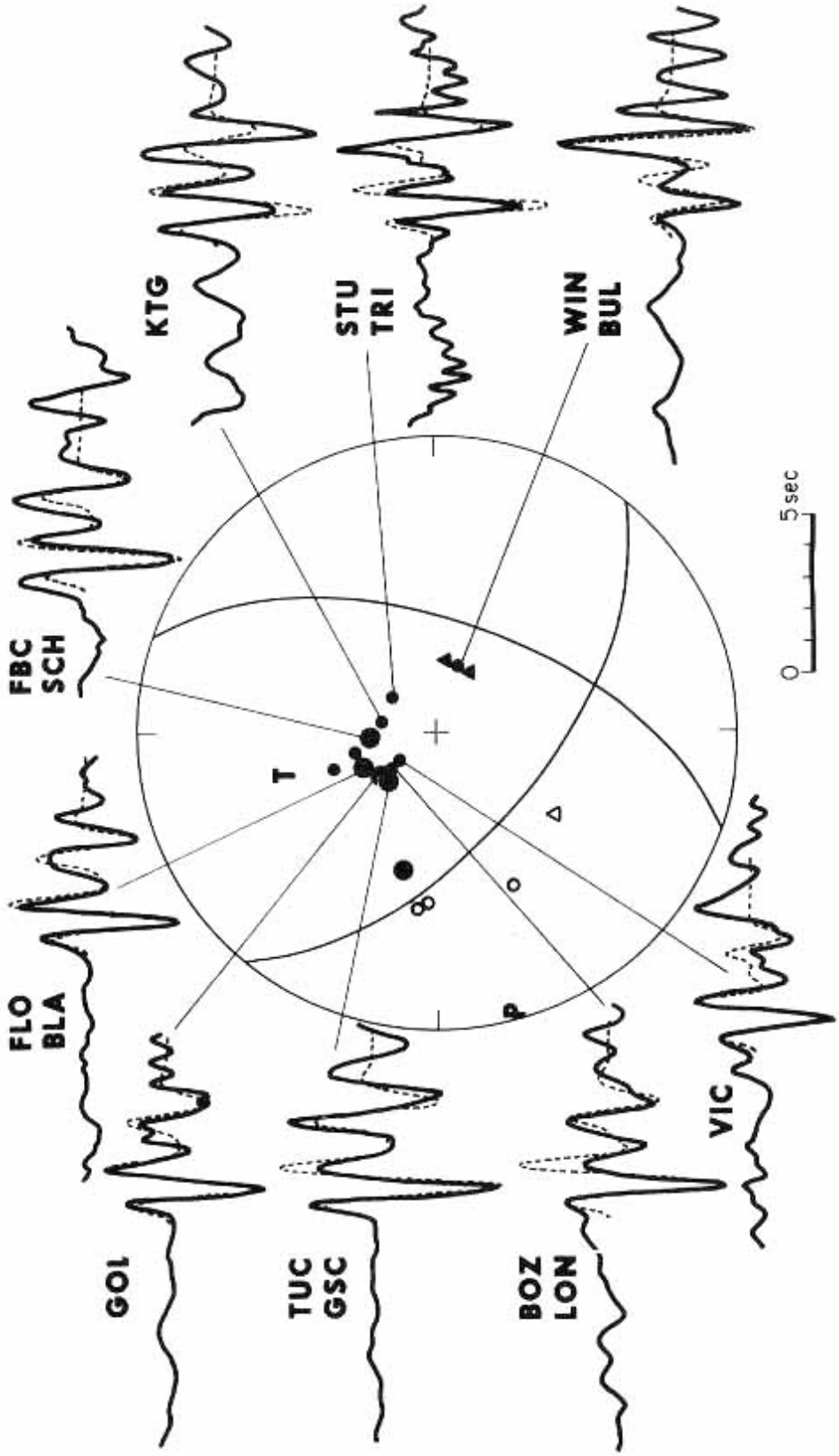

Figure 5. Fault plane solution of Mato Grosso do Sul event of February 13 1964 (No. 4). Stations that plotted very close together in the focal hemisphere (seismograms with two station names) were summed to improve the signal-to-noise ratio. Triangles are polarity data taken from station bulletins; other symbols as in Fig. 2. The nodal plane striking NW–SE was fixed and the other plane was chosen so that synthetic seismograms (dashed lines) best fitted the observed records (solid lines).

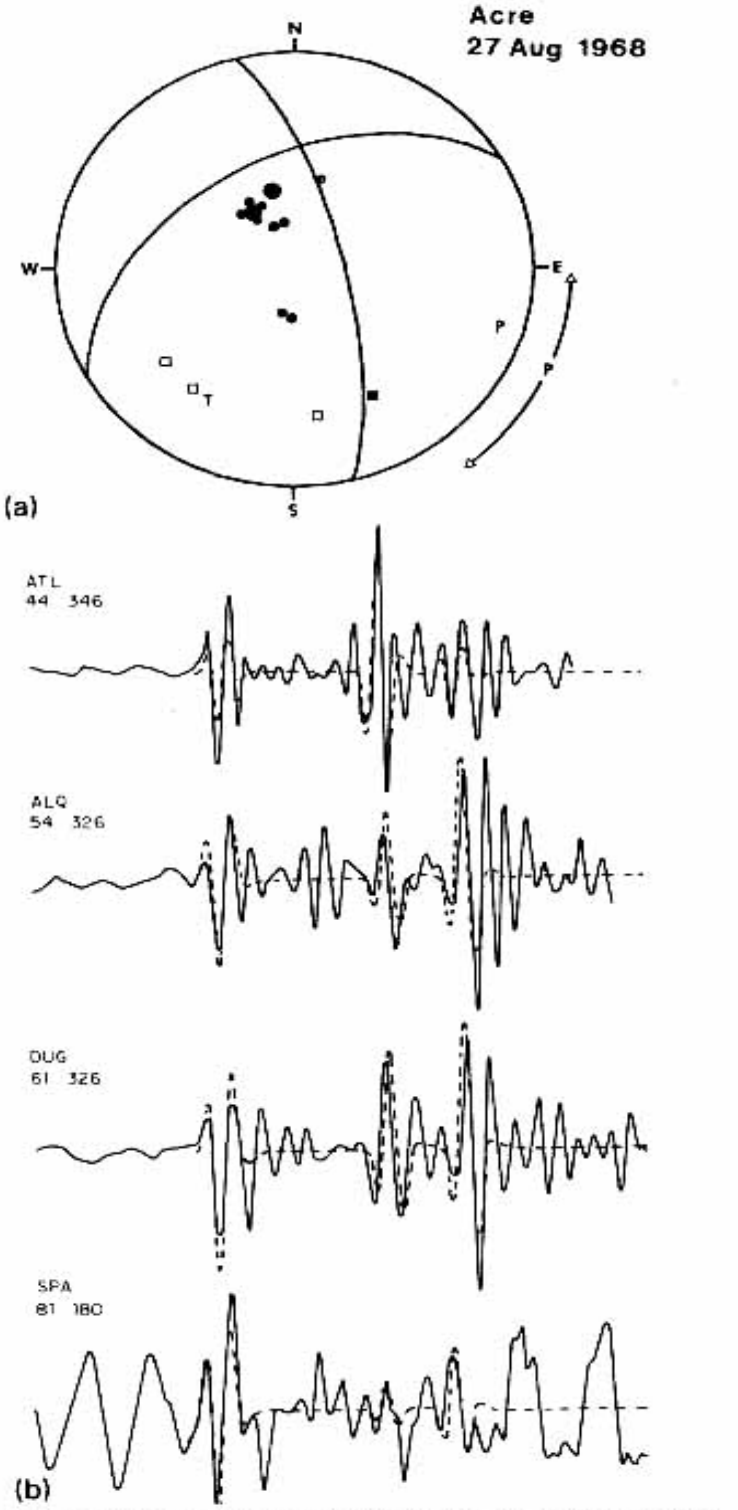

Figure 6. (a) Fault plane solution of Acre event of August 27 1968 (No. 5). Symbols as in Figs 2 and 4. (b) Synthetic seismograms (dashed lines) computed with the fault plane solution of (a) and a half-space model are shown with the observed wavetrains (solid lines). Note the change of polarity of the sP phases between stations ATL and ALQ well reproduced by the PPSP solution.

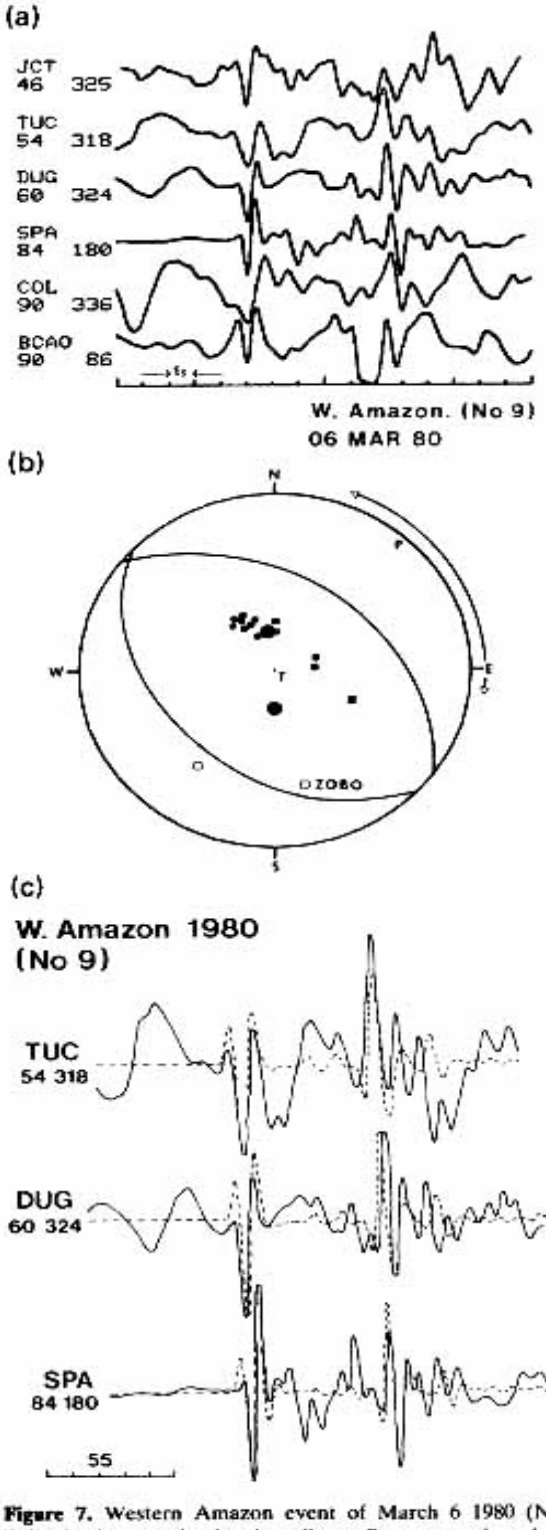

Figure 7. Western Amazon event of March 6 1980 (No. 9). (a) Teleseismic records showing direct P-waves and a depth phase interpreted as pP. Symbols as in Fig. 3. (b) PPSP fault plane solution, $\sigma = 0.18$. Squares are less reliable polarities not used in the PPSP solution. Other symbols as in Figs 2 and 4. (c) Synthetics (dashed lines) computed with a layered crustal model (Table 2).

align the *P*-wave signals remarkably well. The sum of the three records in Fig. 8(b) was obtained after further fine adjustments in the alignment by cross-correlation. The purpose of the initial alignment, using time corrections obtained from other bigger events, was to correctly identify the corresponding peaks and troughs in those three stations. The summed seismograms (Fig. 8a, b) seem to indicate that the *P*-wave first motion in these North American stations was compressional. Records from the French network were also stacked (Fig. 8c) and apparently indicate a dilatational *P*-wave first motion. A station in Africa, BUL, seems to be a dilation (Fig. 8d).

Assuming the polarities above were correctly identified, two hypotheses may be suggested concerning the identification of the depth phase shown in Fig. 8(a), (b): (1) the depth phase was *pP* (hypocentral depth of 16 km) and so *sP* would arrive 2 s later having about the same amplitude as *pP*; (2) the depth phase was *sP* (depth of 12 km) and *pP* would be about 1.5 s earlier with smaller amplitudes. Nodal plane solutions fitting the amplitude ratios for these two hypotheses were sought with the program PPSP. The best solution with hypothesis (1) had a high standard deviation of 0.66. For hypothesis (2) a set of nodal planes could be found with a good standard deviation of 0.22. In the two cases, the clear dilations at a local network about 360 km E of the epicentre were used as further constraints. Therefore, the most probable solution, i.e. the one most consistent with all available information, is the strike–slip mechanism with an ENE-oriented *P*-axis (hypothesis 2) shown in Fig. 8(d). Synthetic seismograms computed with the half-space model show that this strike–slip solution gives a reasonable fit to the available data.

4 DISCUSSION OF THE FOCAL MECHANISM SOLUTIONS

The predominance of reverse and strike–slip mechanisms (Fig. 1) indicates that, as with other mid-plate regions, the continental mid-plate region of the South America plate is in a state of predominantly horizontal compression. The directions of the principal compressive axes, however, are not uniform. The events near the western border of Brazil have approximately E–W-oriented *P*-axes which could be interpreted as being due to the regional lithospheric compression associated with the Nazca–South America plate convergence.

In other parts of Brazil the data are more scattered. Mendiguren & Richter (1978) had proposed that ridge-push from the Mid-Atlantic ridge was a major source of regional stress in Brazil. Richardson *et al.* (1979) have shown that ridge-push seems to be a necessary component of tectonic stress to produce the lithospheric horizontal compression observed in most oceanic intraplate regions (Bergman & Solomon 1980; Wiens & Stein 1984, 1985). Although good evidence for ridge-push has been found in the Antarctic plate 2900 km away from the nearest ridge system (Okal

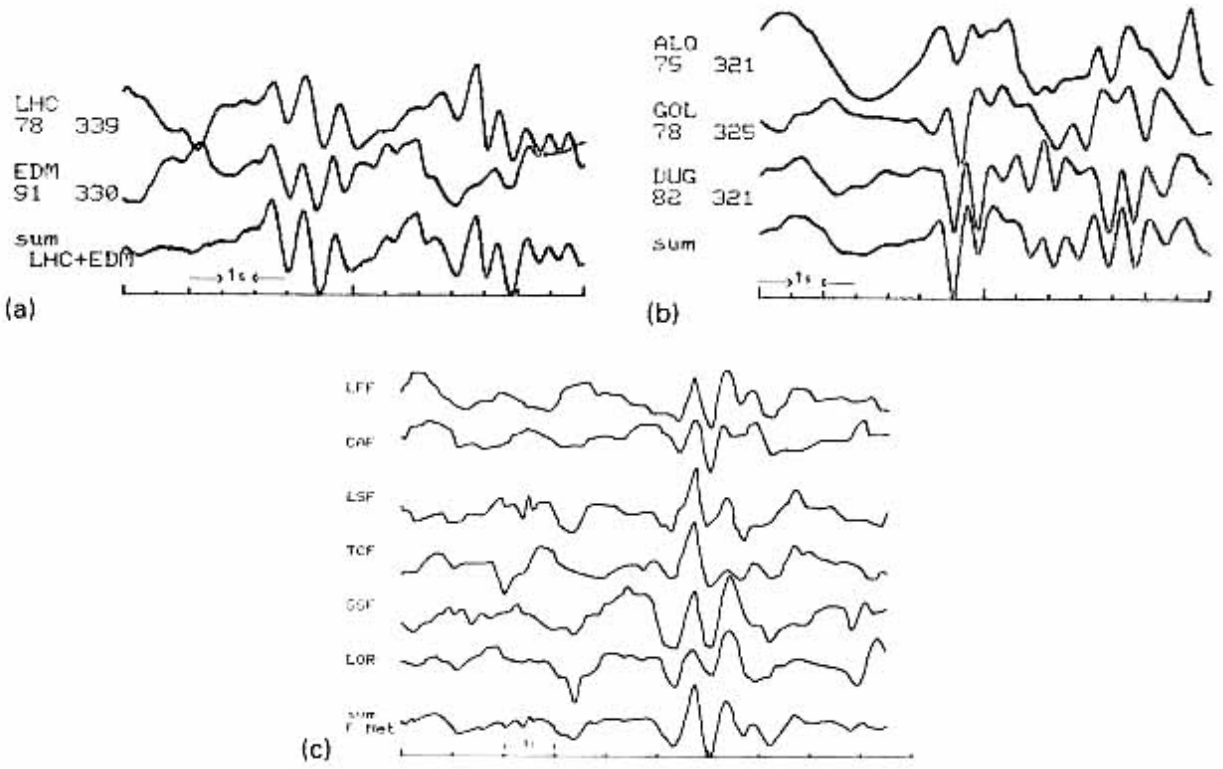

Figure 8. Paraguay event of 1982 April 8 (No. 12). Stacked records of (a) Canadian Network stations; (b) WWSSN North American Stations; (c) French Network stations. (d) Fault plane solution: nodal plane orientations determined with PPSP program ($\sigma = 0.22$); synthetic seismograms (dashed lines) computed with a half-space crustal model.

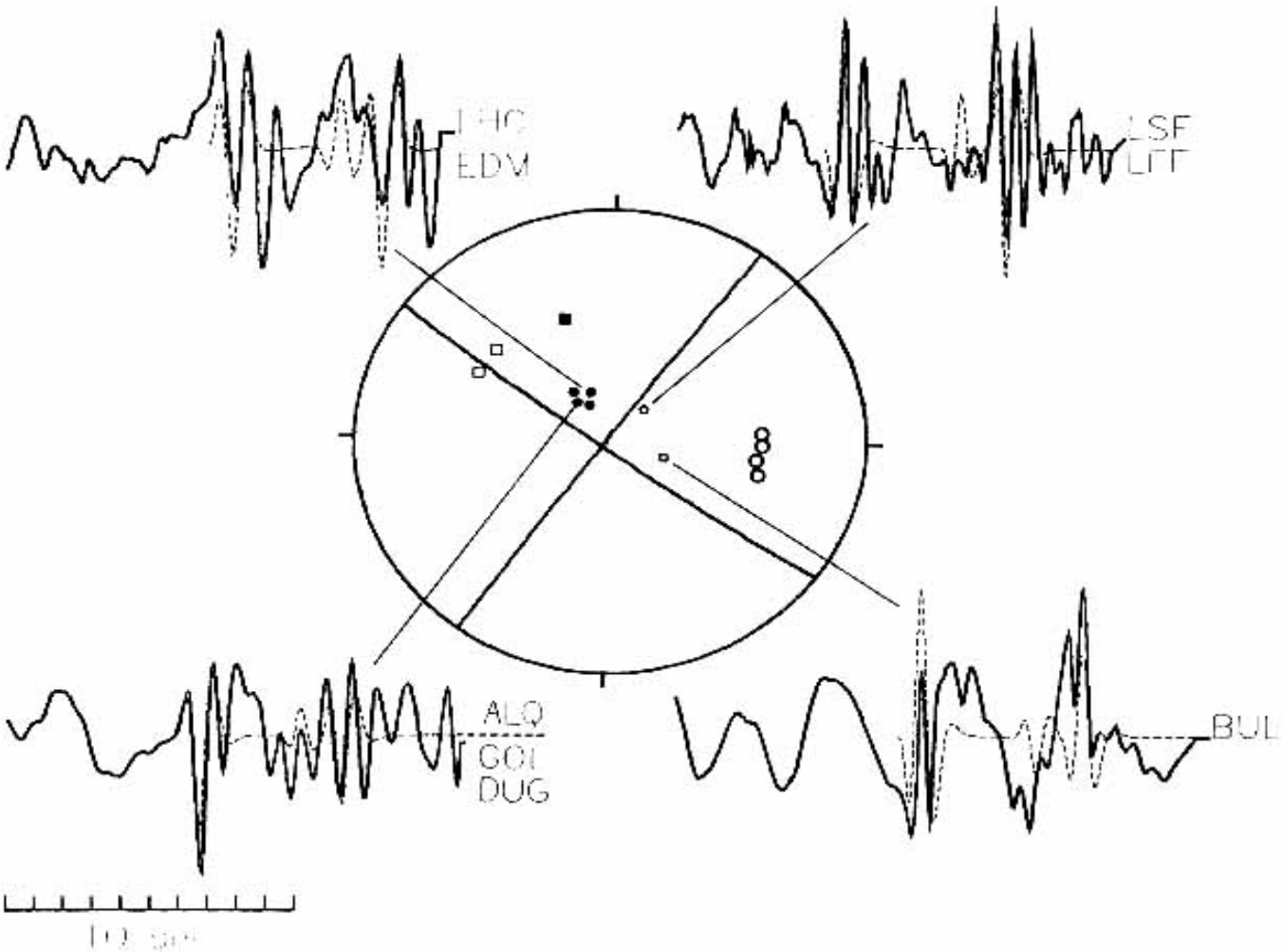

Figure 8 (*Continued*)

1980), in most other oceanic regions the directions of the *P*-axes are rather scattered (Richardson *et al.* 1979; Wiens & Stein 1984) or not sufficiently well defined (Okal 1984) to confirm ridge-push as a major source of tectonic stress inside the plates. Stresses from local sources seem to be comparable with other plate-wide forces in most oceanic plates (Wiens & Stein 1985). In eastern Brazil (Fig. 1) the few available fault plane solutions do not rule out an average E–W-oriented regional compression parallel to the Atlantic spreading direction (which is also about the same direction as South America absolute motion). The events numbered 7 and 8 in SE Brazil are very shallow reservoir-induced events (about 1 km deep) and it is likely that local conditions may be affecting the regional, more uniform stress. Nonetheless, as Assumpção *et al.* (1985) has pointed out, the available data are not yet sufficient to establish the regional stress field in eastern Brazil.

On the other hand, the two events in the central Amazon Basin, with roughly N–S-oriented *P*-axes, may impose some limitations on the range of action of the compressive forces due to the Nazca–South America convergence as well as on the effects of a possible Mid-Atlantic ridge-push.

5 MOMENT AND STRESS DROP

Estimates of seismic moment from Rayleigh waves were attempted for three of the largest events (Table 3 and Fig. 9). For the 1980 event, only periods shorter than about 40 s

Table 3. Results of moment (M_0) and stress drop ($\Delta\sigma$). Range of stress drop values allowed by the uncertainty in the source duration (± 0.2 s); uncertainty in M_0 (about a factor of 2) not taken into account.

Date	M_0 (dyn cm)	Half-duration	Radius (km)	$\Delta\sigma$ (bar)	Range of $\Delta\sigma$ (bar)
14 Dec 1963	1.0×10^{24}	0.70	2.6	25	(15–40)
20 Nov 1980	0.7×10^{24}	0.55	1.5	90	(50–160)
05 Aug 1983	1.0×10^{24}	0.52	1.6	100	(60–200)

were well recorded, which probably accounts for the larger scatter in the amplitudes (Fig. 9b). For the 1983 event, only the six closest stations could be used because of contamination from another earthquake in the Pacific that occurred one hour earlier. Despite the large uncertainties in the M_0 estimates (Fig. 9), they are quite consistent with the m_b vs M_0 relation for mid-plate events (Nuttli 1983) which predicts M_0 ranging from 0.3 to 1.6×10^{24} dyn cm for $5.1 \leq m_b \leq 5.5$.

Estimates of stress drops were made using Brune's (1970) theoretical relationship between seismic moment (M_0), stress drop ($\Delta\sigma$) and the radius of a circular fault (r).

$$\Delta\sigma = \frac{7}{16}\frac{M_0}{r^3}.$$

As no direct determination of the size of the fault was possible (no detailed aftershock studies had been conducted) the radius of the rupture area was estimated from the half-duration of the triangular source-time function used in the P-wave modelling, assuming a rupture velocity of 0.8 times the shear-wave velocity. The resulting stress drops ($\Delta\sigma$) are shown in Table 3. These estimates of stress drops have large uncertainties, mainly because of the errors in the radius of the rupture area due to the trade-off between source duration and apparent attentuation t^*. However, uncertainties of a factor of 2 in M_0 and a factor of 3 or 4 in $\Delta\sigma$ are not uncommon (e.g. Archuleta *et al.* 1982), specially when $\Delta\sigma$ is calculated with the radius of the source estimated from the corner frequency or source duration (Boatwright 1984).

Higher stress drops for large ($M_0 > 10^{25}$) intraplate earthquakes compared with plate-boundary events have often been reported (e.g. Kanamori & Anderson 1975; Scholtz *et al.* 1986), and this can be used as a possible interpretation for differences in m_b vs. M_s relations (Archambeau 1978). Fig. 10 shows that the m_b vs M_s relation for Brazilian events (Table 4) is significantly different from plate-boundary events and similar to other midplate regions. (m_b was determined with the ISC criterion which recommends picking the maximum P amplitude in the first 20 s of the P wave-train; if the NEIS(USGS) criterion, reading in the first 5 s, had been used, m values would be only 0.14 units on average above Nuttli's (1983) relation).

However, confirmation of higher stress drops for moderate Brazilian events is difficult because of the large uncertainties in Table 3. Stress drops in the range 10–100 bar for moderate events ($Mo \approx 10^{23}$ to 10^{24} dyn cm) are not uncommon in plate-boundary regions (e.g. Archuleta *et al.* 1982; Mori 1983; Boatwright 1984; Iio 1986). More accurate, less model-dependent determinations of stress drops are necessary before definite

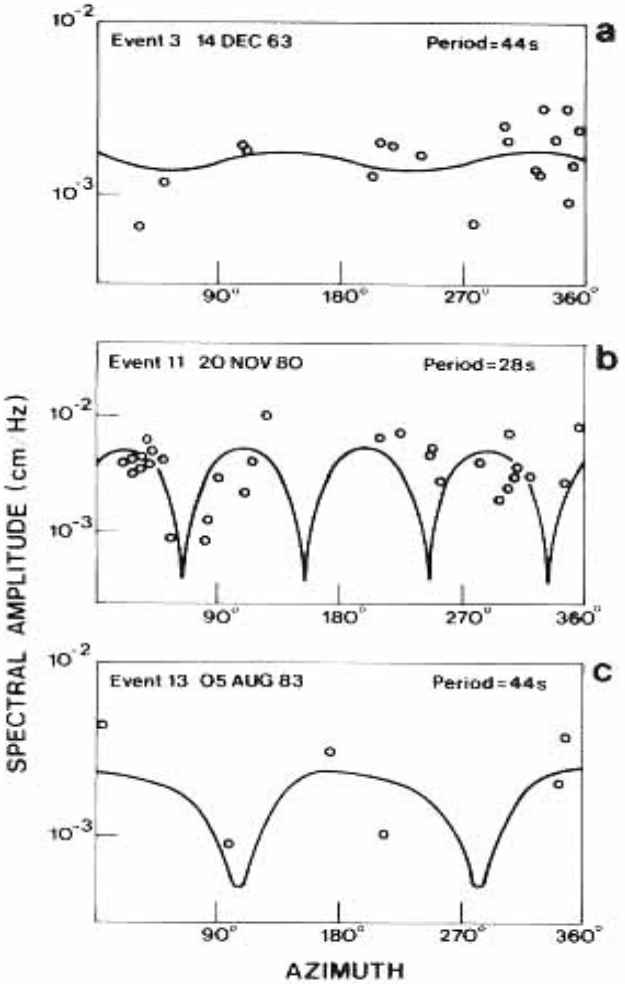

Figure 9. Rayleigh-wave radiation pattern. (a) Spectral amplitudes at 44 s of the Manaus event of 1963 December 14. (b) Spectral amplitudes at 28 s of the Ceará event of 1980 November 20. (c) Spectral amplitudes at 44 s of the Codajás event of 1983 August 5.

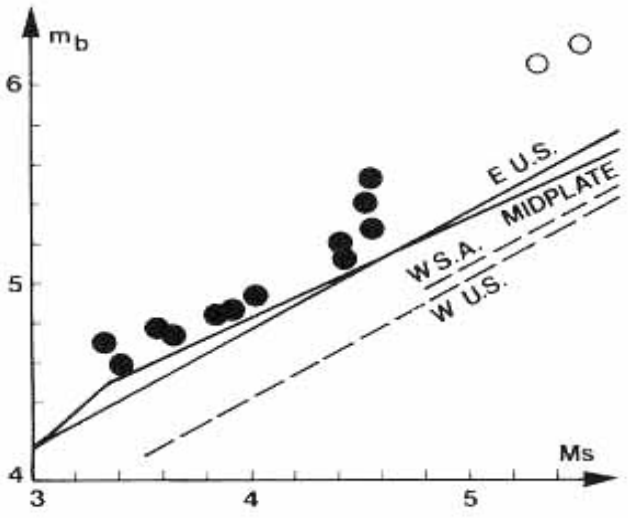

Figure 10. m_b vs. M_s relation for mid-plate events in Brazil and Paraguay (Table 4). E U.S. and W U.S. = Eastern and Western United States, respectively (Chung & Bernreuter 1981). 'Mid-plate' is the semi-theoretical, semi-observational relation for mid-plate events of Nuttli (1983). W S.A. = Western South America (Bueno 1979). Empty circles are less-reliable magnitude values (1955 events in Table 4).

Table 4. Magnitude data used in Fig. 10. First column is event number of Fig. 1 and Table 1.

No.	Date	h min s	Depth (km)	Magnitudes m_b	M_s
01	31.01.1955	05:03:07	N	6.2	5.5
02	01.03.1955	01:46:18	N	6.1	5.3
03	14.12.1963	00:05:42	45	5.1	4.4
04	13.02.1964	11:21:46	5	5.4	4.5
05	27.08.1968	05:17:36	26	4.9	3.9
	24.10.1972	15:36:36	15	4.8	3.8
	22.02.1976	03:24:46	5	4.6	3.4
	02.08.1977	17:45:52	N	4.8	3.6
09	06.03.1980	09:46:18	18	4.8	3.6
10	12.11.1980	21:23:05	N	4.7	3.3
11	20.11.1980	03:29:42	5	5.2	4.4
12	08.04.1982	05:58:52	12	4.9	4.0
13	05.08.1983	06:21:42	23	5.5	4.5
	12.04.1985	14:34:24	24	5.3	4.6

conclusions can be drawn about possible systematic differences between intraplate and plate-boundary events.

ACKNOWLEDGMENTS

This work was carried out while one of the authors (M.A.) was a visiting researcher at Lamont–Doherty Geological Observatory with a grant from CNPq, Brazil, No. 20.0829/83, and later with an American Geophysical Union travel grant. We thank David Simpson and Klaus Jacob for supporting this research. We also thank Leonardo Seeber for many fruitful discussions on intraplate seismicity and Javier Pacheco for the help in computing some synthetic seismograms. This work was supported at Lamont–Doherty through contract NRC 048511302. Lamont–Doherty contribution No. 4239

REFERENCES

Archambeau, C. B., 1978. Estimation of non-hydrostatic stress in the earth by seismic methods: lithospheric stress levels along the Pacific and Nazca plate subduction zones, *Proc. Conf. II, U.S. Geol. Surv., Open-File Rept.* **78–93,** *Methodology for identifying seismic gaps and soon-to-break gaps.*

Archuleta, R. J., Cranswick, E., Mueller, C. & Spudich, P., 1982. Source parameters of the 1980 Mammoth Lakes, California, earthquake sequence. *J. geophys. Res.*, **87,** 4595–4607.

Assumpção, M., Suárez, G. & Veloso, J. A., 1985. Fault plane solutions of intraplate earthquakes in Brazil: some constraints on the regional stress field, *Tectonophysics*, **113,** 283–293.

Bergman, E. A. & Solomon S. C., 1980. Oceanic intraplate earthquakes, implications for local and regional intraplate stress, *J. geophys. Res.*, **85,** 5389–5410.

Bergman, E. A. & Solomon, S. C., 1984. Source mechanisms of earthquakes near mid-ocean ridges from body waveform inversion and implications for the early evolution of oceanic lithosphere, *J. geophys. Res.*, **89,** 11415–11441.

Boatwright, J., 1984. Seismic estimates of stress release. *J. geophys. Res.*, **89,** 6961–6968.

Brune, J. N., 1970. Tectonic stress and the spectra of seismic shear waves, *J. geophys. Res.*, **75,** 4997–5009. (Correction, 1971 *J. geophys. Res.*, **76,** 5002).

Bueno, A. A., 1979. Sismicidade da América do Sul investigada através da relação magnitude-frequência. *MPhil Thesis*, PPPG, Univ. Fed. da Bahia, Brazil, 111pp.

Chen, W. P. & Molnar, P., 1983. Focal depths of intracontinental and intraplate earthquakes and their implications for the thermal and mechanical properties of the lithosphere, *J. geophys. Res.*, **88,** 4183–4214.

Chung, D. H. & Bernreuter, D. L., 1981. Regional relationships among earthquake magnitude scales, *Rev. Geophys. Space Phys.*, **19(4),** 649–663.

Cormier, V. F., 1982. The effect of attenuation on seismic body waves, *Bull. seism. Soc. Am.*, **72,** S169–S200.

Der, Z. A., Rivers, W. D., McElfresh, T. W., O'Donnell, A., Klouda, P. J. & Marshall, M. E., 1982. Worldwide variations in the attenuative properties of the upper mantle as determined from spectral studies of short-period body waves, *Phys. Earth planet. Int.*, **30,** 12–25.

Dziewonski, A. M. & Woodhouse, J. H., 1983. An experiment in systematic study of global seismicity: centroid-moment tensor solutions for 201 moderate and large earthquakes of 1981, *J. geophys. Res.*, **88,** 3247–3271.

Finlayson, D. M., Collins, C. D. N. & Lock, J., 1984. *P*-wave features of the lithosphere under the Eromanga basin, Eastern Australia, including a prominant mid-crustal (Conrad?) discontinuity, *Tectonophys.*, **101,** 267–291.

Godlewski, M. J. C. & West, G. F., 1977. Rayleigh-wave dispersion over the Canadian shield, *Bull. seism. Soc. Am.*, **67,** 771–779.

Iio, Y., 1986. Scaling relation between earthquake size and duration of faulting for shallow earthquakes in seismic moment between 10^{19} and 10^{25} dyne.cm. *J. Phys. Earth*, **34,** 127–169.

Kanamori, H. & Anderson, D. L., 1975. Theoretical basis for some empirical relations in seismology. *Bull. seism. Soc. Am.*, **65,** 1073–1095.

Korhonen, H. & Porkka, M. T., 1981. The structure of the Baltic Shield Region on the basis of DSS and earthquake data, *Pure appl. Geophys.*, **119,** 1093–1099.

Langston, C. A. & Helmberger, D. V., 1975. A procedure for modelling shallow dislocation sources, *Geophys. J. R. astr. Soc.*, **42,** 117–130.

Lay, T. & Helmberger, D. V., 1981. Body wave amplitude patterns and upper mantle attenuation variations across North America. *Geophys. J. R. astr. Soc.*, **66,** 691–726.

McKenzie, D. P., 1969. The relation between fault plane solutions for earthquakes and the directions of the principal stresses, *Bull. seism. Soc. Am.*, **59,** 591–601.

Mendiguren, J. A., 1971. Focal mechanism of a shock in the middle of the Nazca plate, *J. geophys. Res.*, **76,** 3861–3879.

Mendiguren, J. A. & Richter, F. M., 1978. On the origin of compressional intraplate stresses in South America, *Phys. Earth planet. Int.*, **16,** 318–326.

Mendiguren, J. A., 1980. A procedure to resolve areas of different source mechanisms when using the method of composite nodal plane solution, *Bull. seism. Soc. Am.*, **70,** 985–998.

Mori, J., 1983. Dynamic stress drops of moderate earthquakes of the Eastern Aleutians and their relation to a great earthquake. *Bull. seism. Soc. Am.*, **73,** 1077–1097.

Nábělek, J., 1984. Determination of earthquake source parameters from inversion of body waves. *PhD Thesis*, Massachusetts Inst. of Technology, Cambridge, Massachusetts.

Nuttli, O. W., 1983. Average seismic source-parameter relations for mid plate earthquakes, *Bull. seism. Soc. Am.*, **73,** 519–535.

Okal, E. A., 1980. The Bellingshausen Sea earthquake of February 5, 1977: evidence for ridge-generaged compression in the Antarctic plate, *Earth planet. Sci. Lett.*, **46,** 306–310.

Okal, E., 1984. Intraplate seismicity of the southern part of the Pacific plate, *J. geophys. Res.*, **89,** 10053–10071.

Pearce, R. G., 1977. Fault plane solutions using relative amplitudes of *P* and *pP*, *Geophys. J. R. astr. Soc.*, **50,** 381–384.

Pearce, R. G., 1980. Fault plane solutions using relative amplitudes of *P* and surface reflections: further studies, *Geophys. J. R. astr. Soc.*, **60,** 459–487.

Richardson, R. M., Solomon, S. C. & Sleep, N. H., 1976. Intraplate stress as an indicator of plate tectonic driving forces, *J. geophys. Res.*, **81,** 1847–1856.

Richardson, R. M., Solomon, S. C. & Sleep, N. H., 1979. Tectonic stress in the plates, *Rev. Geophys. Space Phys.*, **17,** 981–1019.

Scholtz, C. H., Aviles, C. A. & Wesnousky, S. G., 1986. Scaling

differences between large interplate and intraplate earthquakes. *Bull. seism. Soc. Am.*, **76,** 65–70.

Suárez, G., Molnar, P. & Burchfield, B. C., 1983. Seismicity, fault plane solutions, depth of faulting and active tectonics of the Andes of Peru, Ecuador and Southern Colombia, *J. geophys. Res.*, **88,** 10403–10428.

Sykes, L., 1978. Intraplate seismicity, reactivation of pre-existing zones of weakness, alkaline magmatism, and other tectonism postdating continental fragmentation. *Rev. Geophys. Space Phys.*, **16,** 621–688.

Wiens, D. A. & Stein, S., 1984. Intraplate seismicity and stresses in young oceanic lithosphere, *J. geophys. Res.*, **89,** 11442–11464.

Wiens, D. A. & Stein, S., 1985. Implications of oceanic intraplate seismicity for plate stresses, driving forces and rheology. *Tectonophys.*, **116,** 143–162.

Zoback, M. L. & Zoback, M., 1980. State of stress in the conterminous United States, *J. geophys. Res.*, **85,** 6113–6156.